



HAL
open science

Structural Basis for Galectin-1-dependent Pre-B Cell Receptor (Pre-BCR) Activation

Latifa Elantak, Marion Espeli, Annie Boned, Olivier Bornet, Jeremy Bonzi, Laurent Gauthier, Mikael Feracci, Philippe Roche, Françoise Guerlesquin, Claudine Schiff

► **To cite this version:**

Latifa Elantak, Marion Espeli, Annie Boned, Olivier Bornet, Jeremy Bonzi, et al.. Structural Basis for Galectin-1-dependent Pre-B Cell Receptor (Pre-BCR) Activation. *Journal of Biological Chemistry*, 2012, 287 (53), pp.44703-44713. 10.1074/jbc.m112.395152 . hal-02018151

HAL Id: hal-02018151

<https://hal.science/hal-02018151>

Submitted on 13 Feb 2019

HAL is a multi-disciplinary open access archive for the deposit and dissemination of scientific research documents, whether they are published or not. The documents may come from teaching and research institutions in France or abroad, or from public or private research centers.

L'archive ouverte pluridisciplinaire **HAL**, est destinée au dépôt et à la diffusion de documents scientifiques de niveau recherche, publiés ou non, émanant des établissements d'enseignement et de recherche français ou étrangers, des laboratoires publics ou privés.

Structural Basis for Galectin-1-dependent Pre-B Cell Receptor (Pre-BCR) Activation^{*[5]}

Received for publication, July 3, 2012, and in revised form, October 24, 2012. Published, JBC Papers in Press, November 2, 2012, DOI 10.1074/jbc.M112.395152

Latifa Elantak[‡], Marion Espeli^{§1}, Annie Boned[§], Olivier Bornet[¶], Jeremy Bonzi[‡], Laurent Gauthier^{||}, Mikael Feracci^{**}, Philippe Roche^{‡‡}, Françoise Guerlesquin^{‡2}, and Claudine Schiff^{§3}

From the [‡]Laboratoire d'Ingénierie des Systèmes Macromoléculaires, CNRS UMR7255, Aix-Marseille Université, 13402 Marseille cedex 20, France, the [§]Centre d'Immunologie de Marseille-Luminy, Aix-Marseille Université, UM2, INSERM U1104, CNRS UMR7280, 13288 Marseille cedex 09, France, the [¶]Institut de Microbiologie de la Méditerranée, FR 3479, 13402 Marseille cedex 20, France, ^{||}Innate Pharma, 13276 Marseille, France, the ^{**}Department of Biochemistry, University of Leicester, LE1 9HN Leicester, United Kingdom, and the ^{‡‡}Laboratory of Integrative Structural and Chemical Biology, INSERM U1068, CNRS UMR7258, Aix-Marseille Université, Institut Paoli Calmettes, 13273 Marseille cedex 09, France

Background: Galectin-1 (GAL1) is a ligand for the pre-BCR which is involved in the proliferation and differentiation of normal pre-BII cells.

Results: GAL1-dependent pre-BCR clustering is driven mainly by hydrophobic contacts.

Conclusion: Constitutive and ligand-induced pre-BCR activation can occur in a complementary manner.

Significance: This is the first molecular snapshot of a pre-BCR/ligand interaction that helps pre-BCR clustering and activation.

During B cell differentiation in the bone marrow, the expression and activation of the pre-B cell receptor (pre-BCR) constitute crucial checkpoints for B cell development. Both constitutive and ligand-dependent pre-BCR activation modes have been described. The pre-BCR constitutes an immunoglobulin heavy chain (Ig μ) and a surrogate light chain composed of the invariant $\lambda 5$ and VpreB proteins. We previously showed that galectin-1 (GAL1), produced by bone marrow stromal cells, is a pre-BCR ligand that induces receptor clustering, leading to efficient pre-BII cell proliferation and differentiation. GAL1 interacts with the pre-BCR via the unique region of $\lambda 5$ ($\lambda 5$ -UR). Here, we investigated the solution structure of a minimal $\lambda 5$ -UR motif that interacts with GAL1. This motif adopts a stable helical conformation that docks onto a GAL1 hydrophobic surface adjacent to its carbohydrate binding site. We identified key hydrophobic residues from the $\lambda 5$ -UR as crucial for the interaction with GAL1 and for pre-BCR clustering. These residues involved in GAL1-induced pre-BCR activation are different from those essential for autonomous receptor activation. Overall, our

results indicate that constitutive and ligand-induced pre-BCR activation could occur in a complementary manner.

B cell differentiation in the bone marrow is a highly regulated process. At the pre-BII cell stage, newly generated IgH chains are probed for their ability to interact with surrogate light chains (SLC)⁴ and form a pre-B cell receptor (pre-BCR) that will be expressed at the cell surface (1). The expression of the pre-BCR by pre-BII cells constitutes a critical checkpoint because it controls pre-BII cell proliferation and differentiation (2) and mediates the selection of the Ig μ chain repertoire (3), leading to the counterselection of autoreactive Ig μ chains (4). In mice and humans, mutations in the genes encoding this receptor result in immunodeficiency, leukemia, and autoimmunity.

The pre-BCR is composed of two Ig μ chains, two SLC and the CD79a/b signaling molecules. The crystal structure of the SLC, composed of the $\lambda 5$ and VpreB invariant proteins, exhibits a structure similar to the IgL chain (5). The individuality of $\lambda 5$ and VpreB is contained within their N and C terminus regions, respectively, and they are termed unique regions (URs) because they share no sequence similarity to known proteins. Whereas a portion of the structure of the VpreB-UR 24 amino acids has been solved, no structural data are available for the 52 amino acids forming the $\lambda 5$ -UR (5). Several functional studies have shown that the $\lambda 5$ -UR is essential for pre-BCR activation and function (6–9).

It was first thought that surface expression and co-aggregation of the pre-BCR at the cell surface were sufficient to induce pre-BII cell proliferation and differentiation toward immature B cells (9, 10). However, we reported the formation of an

* This work was supported by grants from the Agence Nationale de la Recherche (ANR-05-BLAN-0035-01), ARC (to M. E.), INSERM, and CNRS and the Fondation pour la Recherche Médicale (to L. E.), the WeNMR Project European FP7 e-Infrastructure grant, Contract 261572, for the use of Web portals, computing, and storage facilities.

[5] This article contains supplemental Tables S1 and S2, Figs. S1–S7, and additional references.

The NMR chemical shifts have been deposited in the BioMagResBank, www.bmrb.wisc.edu (accession no. 18009).

The atomic coordinates and structure factors (code 2KLQ) have been deposited in the Protein Data Bank (<http://www.pdb.org/>).

¹ Present address: University of Cambridge School of Clinical Medicine, Cambridge CB2 2OY, United Kingdom.

² To whom correspondence may be addressed: Laboratoire d'Ingénierie des Systèmes Macromoléculaires, CNRS UMR7255, Aix-Marseille Université, 31 chemin Joseph Aiguier, 13402 Marseille cedex 20, France. Tel.: 33-491-164-379; Fax: 33-491-164-540; E-mail: guerlesquin@imm.cnrs.fr.

³ To whom correspondence may be addressed: Centre d'Immunologie de Marseille-Luminy, Aix-Marseille Université, UM2, INSERM U1104, CNRS UMR7280, case 906, 13288 Marseille cedex 09, France. Tel.: 33-491-269-448; Fax: 33-491-269-430; E-mail: schiff@ciml.univ-mrs.fr.

⁴ The abbreviations used are: SLC, surrogate light chain; CBS, carbohydrate binding site; CRD, carbohydrate recognition domain; GAL1, galectin-1; HSQC, heteronuclear single quantum coherence; PDB, Protein Database; pre-BCR, pre-B cell receptor; TOCSY, total correlated spectroscopy; UR, unique region.

immune developmental synapse between stromal and pre-BII cells where the pre-BCRs relocalize at the cell contact zone, leading to pre-BCR activation and the proliferation and differentiation of pre-BII cells (7, 8, 11). In humans and mice, the formation of the immune synapse takes place through a network of interactions involving galectin-1 (GAL1). During synapse formation, GAL1 binds to the λ 5-UR through a protein/protein interaction and to glycosylated integrins on stromal and pre-BII cells via protein/carbohydrate interactions (8, 11). Consistent with the involvement of GAL1 in pre-BCR relocalization and signaling, GAL1-deficient mice have a defect in pre-BII cell differentiation and proliferation (7). Moreover, GAL1-expressing stromal cells constitute a specific cellular niche for normal pre-BII cells in the bone marrow (12).

GAL1 is a member of the galectin family, which is composed of 15 structurally related proteins with an affinity for β -galactosides (13). They are defined as a shared consensus of amino acid sequence and by their carbohydrate recognition domain (CRD) responsible for β -galactoside binding (14). The carbohydrate binding site (CBS) delineates the CRD pocket where carbohydrates interact. All CRDs possess a remarkably similar fold that is composed of two antiparallel β -sheets of five and six β -strands, arranged in a β -sheet sandwich motif with a jelly roll topology (13–15). GAL1 is implicated in a wide range of biological activities including cell cycle regulation, adhesion, proliferation, and apoptosis (13). Most of the structural studies have focused on GAL1/ β -galactoside interaction, but GAL1 protein partners have also been identified (13). These proteins interact in a carbohydrate-independent manner with GAL1, but no detailed structural data on these interactions have been reported yet.

Given the major impact of GAL1 on pre-BII cell development, it is essential to understand the molecular basis for the GAL1/pre-BCR interaction and to know how pre-BCR relocalization is influenced by this interaction. We now report NMR investigations that reveal the helical structure of the λ 5-UR central region and the structural basis of GAL1/ λ 5-UR interactions that are essential for synapse formation between pre-B and stromal cells.

EXPERIMENTAL PROCEDURES

Cloning, Expression, and Purification of GAL1 Proteins and λ 5-UR Domains; λ 5-UR^{22–45} Peptide Production—The human GAL1 gene sequence was cloned as described previously (11). The oligonucleotides used for this study are listed in [supplemental Table S1](#). The GAL1 mutants were generated using the QuikChange® Site-directed Mutagenesis kit (Stratagene). The production and purification of the GAL1 proteins were performed as described previously (16). For the production of ¹⁵N- or ¹⁵N- and ¹³C-labeled proteins, the cells were grown in M9 minimal medium supplemented with 1 g/liter ¹⁵NH₄Cl and 2 g/liter D-[¹³C]glucose when needed as the sole nitrogen and carbon sources, respectively. The protein production was induced using 1 mM isopropyl- β -D-thiogalactopyranoside when the A₆₀₀ of the cell culture reached 0.7, and the cells were incubated at 37 °C for 3 h and were collected by centrifugation. The unlabeled proteins were produced using the same method, except that LB was used as the culture medium.

For the NMR studies, the gene encoding the human λ 5-UR domain was cloned into a modified pET28a vector (Novagen), which contained an N-terminal His₆ tag fused to a lipoyl domain (17), followed by a tobacco etch virus cleavage site. For the purification of the λ 5-UR, the cells were disrupted using a French press, and the resulting supernatant was clarified by centrifugation at 125,000 \times g. The clarified supernatant was applied to a 5-ml HisTrapTM HP column (GE Healthcare) in accordance with the manufacturer's instructions. After elution, the lipoyl domain was removed from the λ 5-UR by tobacco etch virus protease digestion. The digestion mixture was applied to a HisTrapTM HP column. The flow-through containing the cleaved λ 5-UR was concentrated in an Amicon (Millipore) concentrator, and the samples were applied to a SuperdexTM 75 (10/300GL) gel filtration column (GE Healthcare). The buffer used in the gel filtration experiments was 20 mM sodium phosphate (pH 5.2) (NMR buffer). The chromatographic purifications were performed using the ÄKTA PrimePlus purification system (GE Healthcare).

For the pre-BCR relocalization assays, the gene sequences of the WT and mutant λ 5-UR were cloned as described previously (7) to generate proteins fused to a GST tag. The production and purification of the human His- λ 5-UR-GST were described previously (7). The recombinant proteins were expressed in the BL21-RP strain (Stratagene). The cells were disrupted using a French press, and the resulting supernatant was clarified by centrifugation at 125,000 \times g. The clarified supernatant was purified on glutathione-Sepharose 4B (GE Healthcare) in accordance with the manufacturer's instructions.

The purity and integrity of all proteins were analyzed by SDS-PAGE. The λ 5-UR^{22–45}, λ 5-UR^{22–45}-R27A/R29A, and λ 5-UR^{22–45}-L26A/W30A peptides were chemically synthesized and purchased (Schafer-N, Copenhagen, Denmark).

NMR Experiments—The NMR experiments were performed at 303 K on a Bruker Avance 800 spectrometer equipped with a TXI cryoprobe, or on a Bruker Avance 600 spectrometer equipped with a TCI cryoprobe. The NMR samples contained proteins in 20 mM phosphate buffer (pH 5.2).

The NMR titration was performed using two-dimensional ¹H, ¹⁵N HSQC NMR spectra recorded on ¹⁵N-labeled GAL1 at 0.7 mM concentration (monomer concentration) in the absence and in the presence of increasing amount of λ 5-UR^{22–45} peptide (0.175, 0.35, 0.525, 0.7, 1 mM). The sample buffer contained 20 mM KPO₄ (pH 5.2), 100 mM NaCl, 1.4 mM lactose, 10% D₂O. The chemical shift perturbations for each resonance were calculated using the equation

$$\Delta\delta_{\text{obs}} = ((\Delta\delta_{\text{HN}}^2 + \Delta\delta_{\text{N}}^2/25))^{1/2} \quad (\text{Eq. 1})$$

where $\Delta\delta_{\text{HN}}$ and $\Delta\delta_{\text{N}}$ are, respectively, the proton and nitrogen chemical shifts variation of each residue (18). The dissociation constant (K_D) of GAL1/ λ 5-UR^{22–45} complex formation was obtained by plotting the chemical shift changes from four selected amide cross-peaks (belonging to residues Arg-73, Glu-74, Asn-102, and Phe-106) against the total concentration of the λ 5-UR^{22–45} peptide. Titration curves were fitted with a sigmoidal function, and a K_D was determined for each curves. The final K_D value is the average of the four obtained values.

The lactose binding activity of GAL1 has been determined by recording ^1H , ^{15}N HSQC spectra of 0.2 mM ^{15}N -labeled GAL1 after addition of increasing amount of lactose (0.05, 0.1, 0.15, 0.2, 0.25, 0.3, 0.4, 0.8, 2, and 8 mM). These experiments have been performed either in the absence or in the presence of 3 molar equivalent of $\lambda 5\text{-UR}^{22-45}$ (0.6 mM). Chemical shift variations of His-52 and Trp-68 were calculated using the same equation as above, and K_D values were extracted from the fit of the titration curves.

Effects of $\lambda 5\text{-UR}$ mutations on the complex formation were obtained by NMR chemical shift perturbation mapping on ^{15}N -GAL1 HSQC spectra in the absence and the presence of $\lambda 5\text{-UR}^{22-45}$ mutated peptides. Effects of GAL1 mutations on the complex formation were obtained by NMR chemical shift perturbation mapping performed on mutated ^{15}N -GAL1 proteins in the absence and the presence of $\lambda 5\text{-UR}^{22-45}$.

The two-dimensional ^1H TOCSY and two-dimensional ^1H NOESY experiments were performed on free $\lambda 5\text{-UR}^{22-45}$ for resonance assignment and structure calculation. The resonance assignments and coordinates of the $\lambda 5\text{-UR}^{22-45}$ domain structure have been deposited in the BioMagResBank (accession no. 18009) and the Protein Database (PDB ID code 2LKQ), respectively. The two-dimensional ^{15}N , ^{13}C -filtered NOESY spectra were recorded on the $\lambda 5\text{-UR}^{22-45}/^{15}\text{N}$, ^{13}C -GAL1 sample at a ratio of 1.25/1 for calculation of the bound $\lambda 5\text{-UR}^{22-45}$ structure. The backbone sequential resonances of ^{15}N , ^{13}C -labeled GAL1 bound to $\lambda 5\text{-UR}^{22-45}$ were assigned using three-dimensional HNCA, HN(CO)CA, CBCA(CO)NH experiments, and side chain resonances were assigned using three-dimensional HCCH-TOCSY experiments. The intermolecular NOEs between the $\lambda 5\text{-UR}^{22-45}$ and ^{15}N , ^{13}C -GAL1 were obtained using two-dimensional ^{15}N , ^{13}C half-filtered NOESY experiments.

The structures of the free and bound $\lambda 5\text{-UR}^{22-45}$ peptides were calculated using the CYANA software. Next, these structures were water-refined in a minimization run using the SANDER module of AMBER 9.0 software (19). The quality of each structure was assessed using the PROCHECK-NMR program (20). The structural model of the complex was calculated using the HADDOCK program (21).

Immunofluorescence Imaging—The co-cultures of the Nalm6 pre-B cells and OP9 stromal cells were performed as described previously (7), in the presence or the absence of the indicated His- $\lambda 5\text{-UR}$ -GST proteins (40 $\mu\text{g}/\text{ml}$). After fixation, the cells were stained with goat anti-human IgM antibodies (Southern Biotech) and were visualized using AF555-labeled donkey anti-goat IgG (Invitrogen) or rabbit anti-GAL1 antiserum (8) and AF488-labeled goat anti-rabbit IgG (Invitrogen). The cells were mounted and analyzed on a LSM510 Carl Zeiss confocal microscope. The slides were scanned by differential interferential contrast imaging, and 100–380 pre-B cells in contact with stromal cells were examined further for their surface fluorescence distribution. The inhibition of pre-BCR relocalization was calculated as described previously (7). The S.D. values were calculated from three independent experiments. The p values were determined using the Mann-Whitney unpaired test with a risk of 5%, n.s = not significant; *, $p \leq 0.05$; **, $p \leq 0.01$; ***, $p \leq 0.001$.

RESULTS

The $\lambda 5\text{-UR}^{22-45}$ Fragment Contains the Determinants Required for GAL1 Binding—We have shown previously that the GAL1-interacting site on the pre-BCR is located within the $\lambda 5\text{-UR}$ domain (7, 8). The theoretical predictions (supplemental Fig. S1 and Ref. 22) indicate that the full-length $\lambda 5\text{-UR}$ (45 amino acids from Ser-8 to Ser-52) contains a potential short α -helix in its middle region (Ser-28 to Arg-37) whereas the rest of the domain is unfolded (supplemental Fig. S1C). In agreement, the $\lambda 5\text{-UR}$ CD spectrum (supplemental Fig. S1D) exhibits a weak shoulder in the 209–222-nm region corresponding to helical structures, and a strong negative band near 200 nm represents random coil conformations. This type of spectrum is typical of proteins having a low level of α -helical structures.

To investigate whether this potential small helical region of $\lambda 5\text{-UR}$ constitutes a sufficient binding epitope for GAL1, a 24-mer peptide covering amino acids 22–45 ($\lambda 5\text{-UR}^{22-45}$) was chemically synthesized and tested for binding to GAL1 using NMR spectroscopy. An NMR titration was performed by recording two-dimensional ^1H , ^{15}N HSQC spectra of the ^{15}N -labeled GAL1 bound to lactose in the absence and the presence of increasing amount of the $\lambda 5\text{-UR}^{22-45}$ peptide (Fig. 1A). We monitored the perturbations in the NMR signal of the ^{15}N -GAL1 homodimer (28 kDa), making use of the previously published resonance assignment of human GAL1 bound to lactose (23). Significant variations were observed implying that a specific interaction occurred. The binding was in the fast exchange regime on the NMR chemical shift time scale and indicated a 1:1 complex stoichiometry (one $\lambda 5\text{-UR}$ /GAL1 monomer). Chemical shift perturbations (Fig. 1B) of four GAL1 residues (Arg-73, Glu-74, Asp-102, Phe-106) chosen among the peaks experiencing the largest variations were plotted against $\lambda 5\text{-UR}^{22-45}$ concentration (Fig. 1C). The average K_D value derived from the fit of the curves corresponds to $310 \pm 65 \mu\text{M}$.

Upon $\lambda 5\text{-UR}^{22-45}$ binding, GAL1 residues experiencing significant chemical shift displacements are localized in the CBS (including strands $\beta 3$, $\beta 4$, and $\beta 5$) and on a surface adjacent to this region (including strands $\beta 6$, $\beta 7$, and $\beta 9$) (Fig. 1, D and E). The same regions of GAL1, localized at its side and back face, undergo chemical shift variations upon $\lambda 5\text{-UR}^{22-45}$ addition in the absence of lactose (Fig. 2, A and B, and supplemental Fig. S2A). These observations indicate that $\lambda 5\text{-UR}^{22-45}$ uses the same mode of binding to GAL1 in the absence and in the presence of lactose.

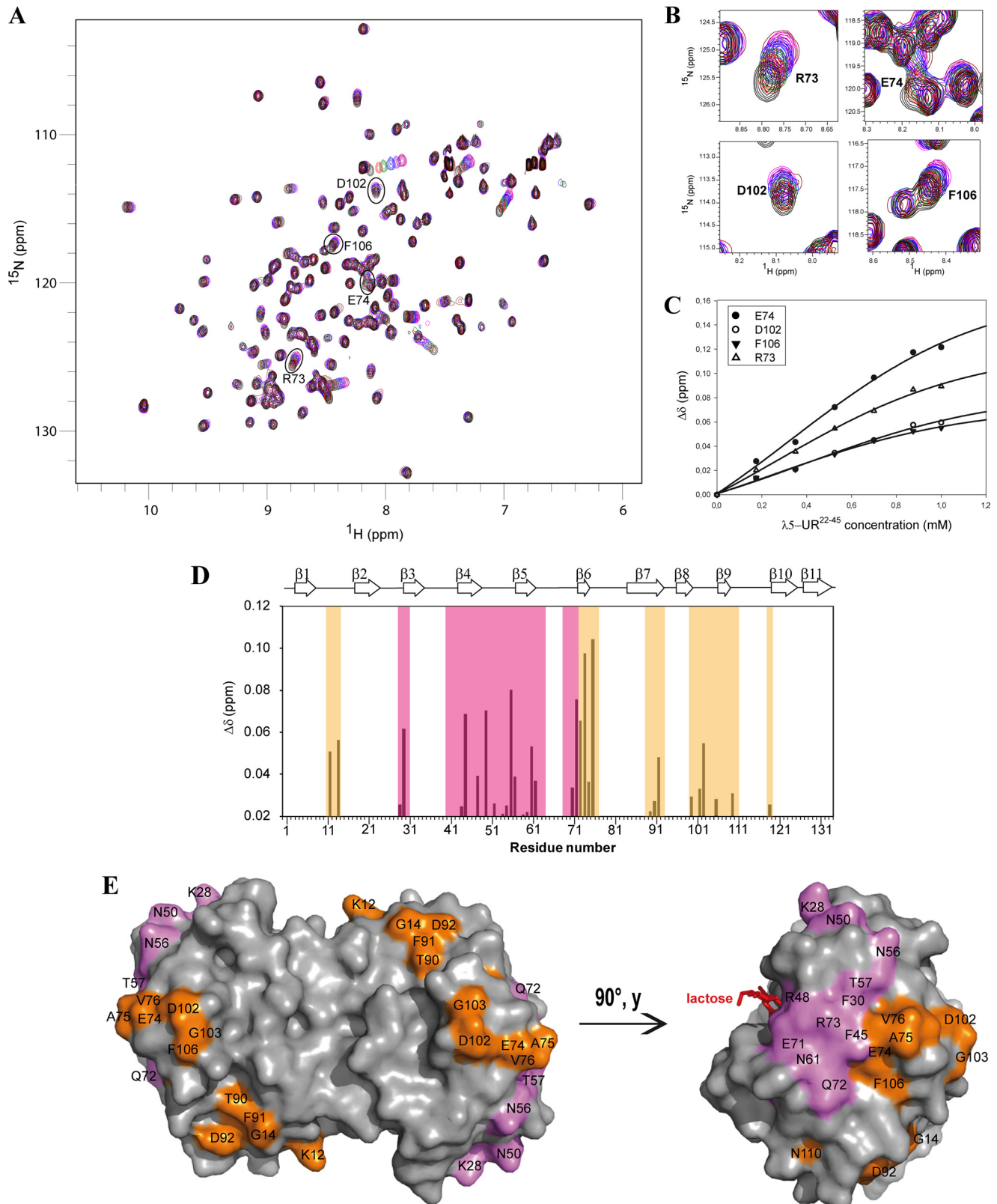
The same chemical shift perturbation mapping experiment was performed using ^{15}N -labeled GAL1 and the full-length $\lambda 5\text{-UR}$ instead of the $\lambda 5\text{-UR}^{22-45}$ peptide (Fig. 2C and supplemental Fig. S2B). Once again, similar effects were observed with the same regions of GAL1 experiencing changes upon $\lambda 5\text{-UR}$ binding (compare Fig. 2, C with A). This result indicates that the $\lambda 5\text{-UR}^{22-45}$ fragment uses the same mode of binding to GAL1 as the full-length $\lambda 5\text{-UR}$ and therefore contains the sequence and structure determinants required for GAL1 binding.

The $\lambda 5\text{-UR}^{22-45}$ Contains an α -Helix Structure in Solution and in Complex with GAL1—To verify the presence of an α -helical structure within $\lambda 5\text{-UR}^{22-45}$, first we solved the solution structure of the free $\lambda 5\text{-UR}^{22-45}$ peptide using homo-

Galectin-1/Pre-BCR Interaction

nuclear NMR spectroscopy. Using the CYANA software and based on 231 distance restraints among which 49 were medium range (supplemental Fig. S3A), 100 structures were calculated, and the 20 lowest energy structures are shown in Fig. 3A. The structural statistics (supplemental Table S2) demonstrate a well

defined structure with low pairwise root mean square deviation values of $1.3 \pm 0.08 \text{ \AA}$ ($0.89 \pm 0.07 \text{ \AA}$ for residues 25–41). The structure of the free $\lambda 5$ -UR^{22–45} peptide reveals the presence of a short 10-amino acid α -helix (from residues Arg-29 to Ser-39) among the 24 residues of the peptide (Fig. 3A), whereas the N-



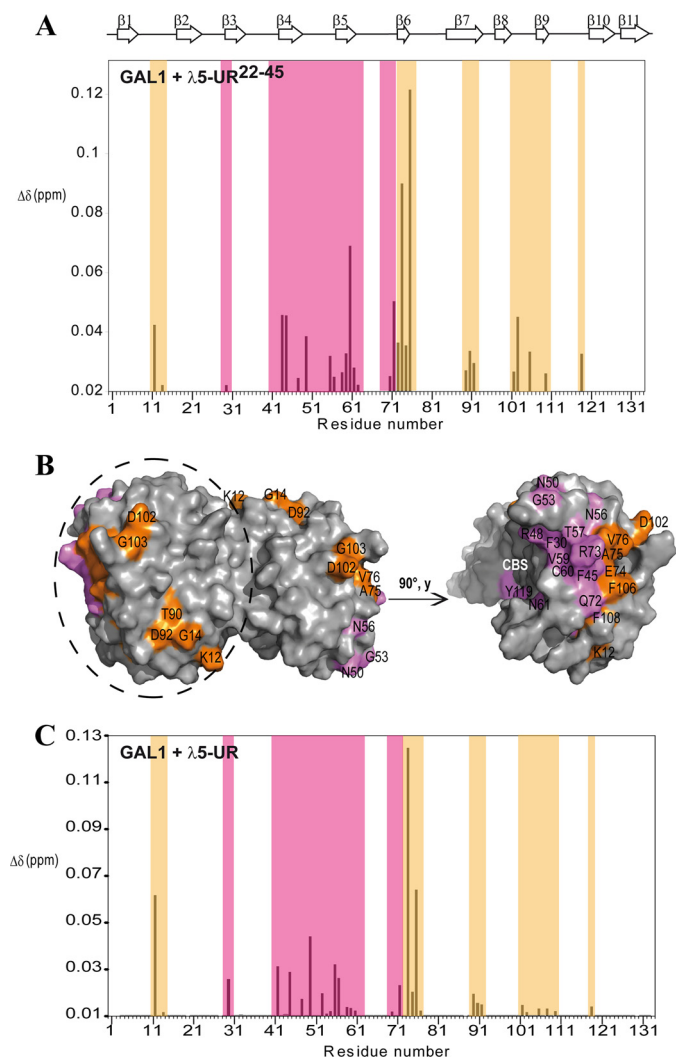


FIGURE 2. $\lambda 5$ -UR^{22–45} and $\lambda 5$ -UR interaction sites on GAL1. **A**, normalized chemical shift perturbations induced upon addition of 1 molar equivalent of $\lambda 5$ -UR^{22–45} to ¹⁵N-labeled GAL1 in the absence of lactose, as monitored in ¹H,¹⁵N HSQC spectra (supplemental Fig. S2A). The plot is color-coded according to the location of the residues showing the largest variations on GAL1 structure (orange, side and back face; pink, CBS). The secondary structures of GAL1 are shown above the plot. **B**, GAL1 chemical shift perturbations upon addition of $\lambda 5$ -UR^{22–45} mapped onto the surface representation of the GAL1 dimer structure (PDB ID code 2KM2 (24)). The residues are labeled and color-coded as in A. A single GAL1 monomer is circled. **C**, normalized chemical shift changes induced upon addition of 1 molar equivalent of $\lambda 5$ -UR to ¹⁵N-labeled GAL1 (0.1 mM), as monitored in ¹H,¹⁵N HSQC spectra (supplemental Fig. S2B). The plot is color-coded as in A.

and C-terminal residues flanking the helix are not structured in agreement with the theoretical predictions (supplemental Fig. S1C) (6).

The structure of the $\lambda 5$ -UR^{22–45} peptide bound to GAL1 was then investigated using a ¹⁵N,¹³C-filtered NOESY spectrum

recorded on the $\lambda 5$ -UR^{22–45}/¹⁵N,¹³C-labeled GAL1 sample. In this experiment, only the resonances belonging to the unlabeled protein (*i.e.* $\lambda 5$ -UR^{22–45}) are detected. After proton resonances assignment, NOE-derived distance restraints were collected (supplemental Fig. S3B and supplemental Table S2). The structure calculations performed confirmed the existence of the helix when $\lambda 5$ -UR^{22–45} is bound to GAL1 (Fig. 3B) as illustrated by the conservation of the helix-forming restraints (Fig. 3C). Thus, a short α -helix within the $\lambda 5$ -UR^{22–45} preexists in solution and its structure is conserved upon binding to GAL1. We next investigated whether this helix plays a crucial role in GAL1 binding.

$\lambda 5$ -UR^{22–45} Binds to GAL1 on a Surface Close to the CBS and Induces Changes in GAL1 Lactose Binding Activity—To gain further insight into the possible modes of interaction of the $\lambda 5$ -UR^{22–45} peptide with GAL1, a structural model of the complex was calculated using the HADDOCK program (21). We used the 10 best NMR structures of the $\lambda 5$ -UR^{22–45} peptide and the lowest energy NMR structure of the human GAL1 (24). On the basis of the $\lambda 5$ -UR^{22–45} peptide and GAL1 resonance assignments that we performed on the complexed forms, 10 intermolecular NOE restraints have been assigned in the ¹⁵N,¹³C half-filtered NOESY spectrum recorded on the ¹⁵N,¹³C GAL1/ $\lambda 5$ -UR^{22–45} complex (supplemental Fig. S4). These intermolecular NOE restraints have been used to restrain the dockings. The GAL1/ $\lambda 5$ -UR^{22–45} complex was a good candidate for this structure calculation strategy because neither protein undergoes large scale conformational changes upon complex formation as seen by the limited extent of chemical shift perturbations (Fig. 1D). The docking calculations yielded a dominant cluster of 182 solutions of the 200 solutions obtained.

The structural model (Fig. 4A) shows that the $\lambda 5$ -UR^{22–45} peptide binds to a surface localized at the interface between the two GAL1 β -sheets near the CBS (Fig. 4B). This surface corresponds to the area adjacent to the CBS highlighted by the chemical shift perturbation mapping (Fig. 1E, orange surface). The close proximity of the CBS and of the $\lambda 5$ -UR^{22–45} interacting surface on GAL1 led us to investigate the lactose binding activity of GAL1 in the absence and in the presence of $\lambda 5$ -UR^{22–45} peptide, using NMR chemical shift perturbations. As shown in the ¹H,¹⁵N HSQC spectra (Fig. 5, A and B), chemical shift variations upon lactose addition are significantly modified when $\lambda 5$ -UR^{22–45} is present. This result indicates that lactose affinity for GAL1 is significantly reduced when GAL1 is bound to $\lambda 5$ -UR^{22–45}. To illustrate these changes we focused on two GAL1 residues involved in key interactions with lactose, His-52, and Trp-68 (Fig. 5C). Both titration curves show lower chemical shift variations in the presence of $\lambda 5$ -UR^{22–45}. K_D evaluations in these experimental conditions led to a value of

FIGURE 1. NMR titration of GAL1/ $\lambda 5$ -UR^{22–45} interaction. **A**, ¹H,¹⁵N HSQC spectra of ¹⁵N-labeled GAL1 (0.7 mM) in the absence (black) and in the presence of unlabeled $\lambda 5$ -UR^{22–45} peptide at a concentration of 0.175 mM (red), 0.35 mM (green), 0.525 mM (blue), 0.7 mM (violet), 0.875 mM (magenta), and 1 mM (maroon). Spectra were recorded on a 600-MHz spectrometer at 303 K in 20 mM KPO₄ (pH 5.2), 100 mM NaCl, 1.4 mM lactose, 10% D₂O. **B**, enlarged views of the ¹H,¹⁵N HSQC spectra for Arg-73, Glu-74, Asp-102, and Phe-106 peaks. **C**, plot of the chemical shift variations of Arg-73, Glu-74, Asp-102, and Phe-106 proton amide against $\lambda 5$ -UR^{22–45} concentration. Titration curves were fitted with a sigmoidal function. The K_D derived from the fit of the curves corresponds to 310 ± 65 μ M. **D**, normalized chemical shift perturbations monitored in ¹H,¹⁵N HSQC spectra of ¹⁵N-labeled GAL1 with a 2 molar excess of lactose following the addition of $\lambda 5$ -UR^{22–45} (1 molar equivalent). The plot is color-coded according to the location of the residues (orange, side and back face; pink, CBS). The secondary structures of GAL1 are shown above the plot. **E**, GAL1 ¹H,¹⁵N HSQC chemical shift perturbations mapped onto the GAL1 dimer structure bound to lactose (PDB ID code 1GZW (15)) following the addition of the $\lambda 5$ -UR^{22–45}. The residues exhibiting significant chemical shift variations in the presence of the $\lambda 5$ -UR^{22–45} are labeled and colored according to the color code used in D. From left to right, back view, side view.

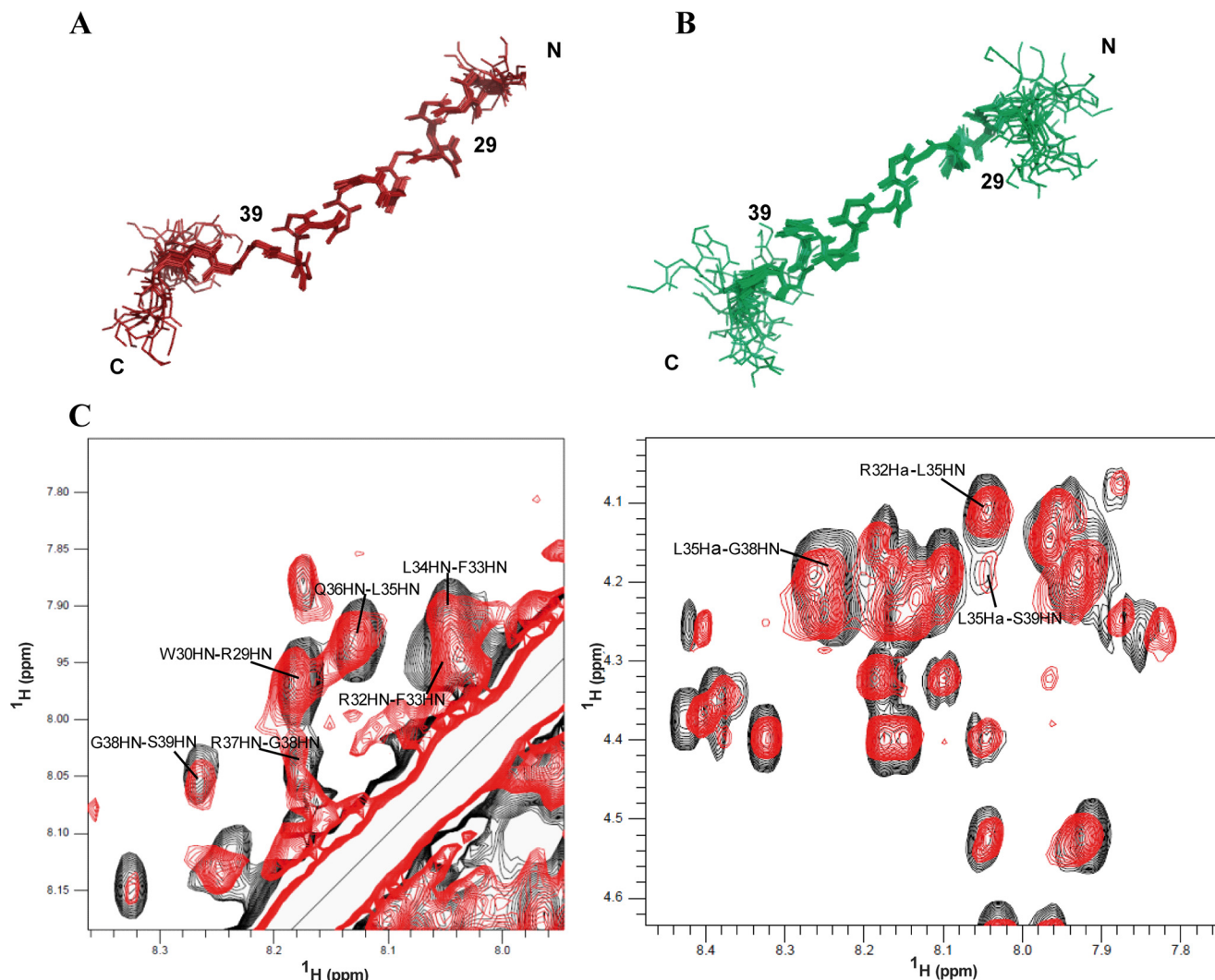


FIGURE 3. **Structure of $\lambda 5$ -UR²²⁻⁴⁵ free and bound to GAL1.** *A* and *B*, ensemble of the backbone traces of the 20 superimposed lowest energy NMR structures of $\lambda 5$ -UR²²⁻⁴⁵ (*A*) and of $\lambda 5$ -UR²²⁻⁴⁵ bound to GAL1 (*B*). *C*, superimposition of regions extracted from two-dimensional ¹H NOESY spectra recorded on $\lambda 5$ -UR²²⁻⁴⁵ (*red spectrum*) and two-dimensional ¹³C, ¹⁵N-filtered NOESY recorded on ¹³C, ¹⁵N-GAL1 complexed to $\lambda 5$ -UR²²⁻⁴⁵ (*black spectrum*). Some correlations indicative of a α -helix conformation are labeled. *Left panel* zooms on an amide proton region; *right panel* presents some proton amide/ α -proton correlations.

0.907 ± 0.061 mM in the absence of the peptide and of 3.7 ± 0.3 mM in the presence of the peptide. Therefore, peptide binding to GAL1 induces a 4-fold decrease in the lactose binding activity of GAL1.

Structural Analysis of the GAL1/ $\lambda 5$ -UR²²⁻⁴⁵ Complex Highlights Hydrophobic and Electrostatic Interactions—As shown in Fig. 4, *B* and *C*, the entire length of the $\lambda 5$ -UR²²⁻⁴⁵ α -helix (residues Arg-29 to Ser-39) is involved in the direct interaction with GAL1 in a completely buried surface area of 926.1 Å². Although the binding surface is mostly hydrophobic, it is surrounded by a number of charged residues. The GAL1-interacting surface consists primarily of residues from the $\beta 9$ strand (Tyr-104, Glu-105, Phe-106, and Lys-107) with a number of residues from the $\beta 6$ strand (Glu-74), loop $\beta 6$ – $\beta 7$ (Val-76), loop $\beta 7$ – $\beta 8$ (Asp-102), and loop $\beta 9$ – $\beta 10$ (Asn-110). The Trp-30 side chain of the $\lambda 5$ -UR²²⁻⁴⁵ peptide projects toward the center of the hydrophobic surface presented by GAL1 and is totally buried. The Trp-30 aromatic ring is surrounded by a triad of hydrophobic side chains from GAL1 (Val-76, Tyr-104,

and Phe-106) among which the Phe-106 aromatic ring is directly facing the Trp-30 ring of the $\lambda 5$ -UR²²⁻⁴⁵, thus contributing strongly to the hydrophobic interactions within the complex (Fig. 4*C*). Moreover, the additional aliphatic side chains, such as the Leu-26 of $\lambda 5$ -UR²²⁻⁴⁵, project along the peptide creating a hydrophobic surface on the helix, which complements the hydrophobic surface of GAL1 (Fig. 4*C*). Surprisingly, despite the high arginine content of the $\lambda 5$ -UR²²⁻⁴⁵ peptide, only Arg-27 and Arg-29 in the N-terminal part of the $\lambda 5$ -UR²²⁻⁴⁵ peptide are found engaged in salt bridges with the Asp-102 and Glu-74 acidic residues of GAL1, respectively (Fig. 4*B*). These acidic residues are located adjacent to, but on both sides of, the GAL1 hydrophobic surface (Fig. 4*C*). Therefore, these structural data reveal a dual mode for GAL1 binding to the $\lambda 5$ -UR²²⁻⁴⁵ peptide, which involves both hydrophobic and electrostatic interactions.

Hydrophobic Interactions Are Essential for Relocalization of the Pre-BCR at the Pre-B/Stromal Cell Synapse—The clustering of pre-BCRs at the surface of the pre-B-II cells is a prerequisite to

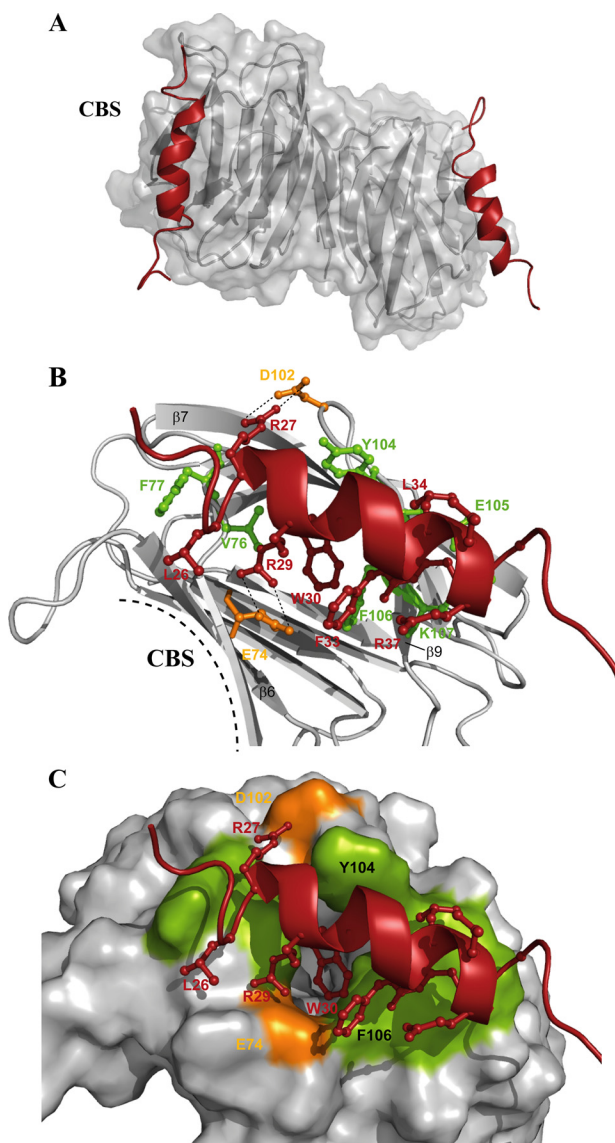


FIGURE 4. Structural model of the $\lambda 5$ -UR²²⁻⁴⁵/GAL1 complex. *A*, representation of the lowest energy structure of GAL1 bound to $\lambda 5$ -UR²²⁻⁴⁵. GAL1 is displayed as a semitransparent solvent-accessible surface with a ribbon model displayed below the surface. The GAL1 dimer is colored gray, and $\lambda 5$ -UR²²⁻⁴⁵ is colored in red ribbon. *B*, ribbon view of the $\lambda 5$ -UR²²⁻⁴⁵/GAL1 complex with the side chains of the contacting residues shown and labeled. The GAL1 hydrophobic and acidic contacting residues are colored green and orange, respectively. The $\lambda 5$ -UR²²⁻⁴⁵ residues are colored red, and the electrostatic interactions are represented as dashed lines. *C*, magnification of the GAL1 interaction surface (same orientation as in *B*) highlighting the hydrophobic (green) and electrostatic (orange) residues contacting the $\lambda 5$ -UR²²⁻⁴⁵. The mutated residues are labeled.

their activation, leading to the trans-phosphorylation of the I α / β molecules. Receptor clustering may occur in an autonomous manner (9) and/or may be induced by the bone marrow microenvironment through the GAL1/pre-BCR interaction, leading to pre-BCR relocalization (8). Based on the structural model of the GAL1/ $\lambda 5$ -UR²²⁻⁴⁵ complex, we tested at a cellular level the contribution of hydrophobic and electrostatic interactions on the pre-BCR relocalization process using full-length $\lambda 5$ -UR and two double $\lambda 5$ -UR mutants ($\lambda 5$ -UR-L26A/W30A and $\lambda 5$ -UR-R27A/R29A). The pre-B cells were co-cultured with stromal cells, and pre-BCR and GAL1 clustering was

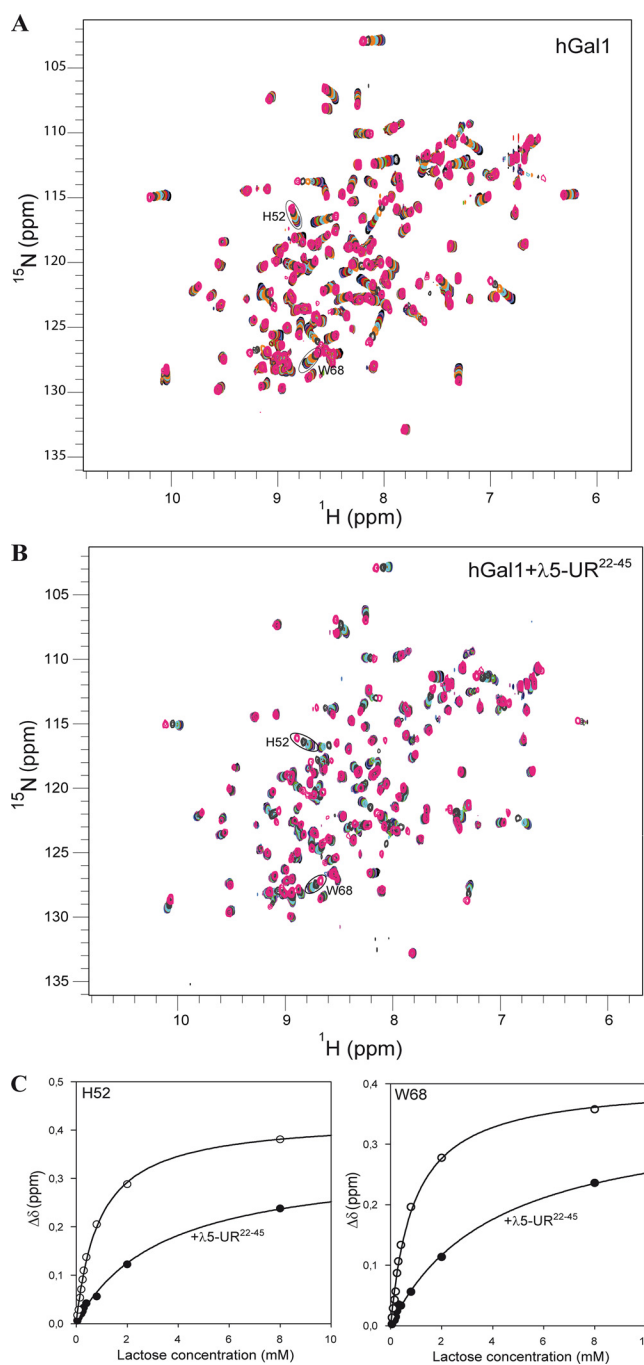


FIGURE 5. Lactose binding activity of GAL1 free and bound to $\lambda 5$ -UR²²⁻⁴⁵. *A* and *B*, ¹H,¹⁵N HSQC spectra of ¹⁵N-labeled GAL1 (0.2 mM concentration) upon addition of increasing amount of lactose in the absence (*A*) and in the presence (*B*) of 3 molar equivalent of $\lambda 5$ -UR²²⁻⁴⁵. Spectra were recorded with 0 (black), 0.05 (skyblue), 0.1 (magenta), 0.15 (navy), 0.2 (red), 0.25 (lime), 0.3 (maroon), 0.4 (cyan), 0.8 (orange), 2 (dark gray), and 8 (pink) mM lactose. *C*, lactose titration curves in the absence (○) and in the presence (●) of $\lambda 5$ -UR²²⁻⁴⁵ for His-52 and Trp-68 are shown. Chemical shift variations differences are plotted against lactose concentration.

observed at the pre-B/stromal cell contact site using confocal microscopy (Fig. 6A). As reported previously, the addition of the full-length $\lambda 5$ -UR into co-cultures inhibits the relocalization process by 25% (7). In contrast, the addition of the $\lambda 5$ -UR-L26A/W30A mutant has no effect on the pre-BCR relocalization process compared with the native $\lambda 5$ -UR (Fig. 6B). This result is significant (p value = 0.018), implying that hydropho-

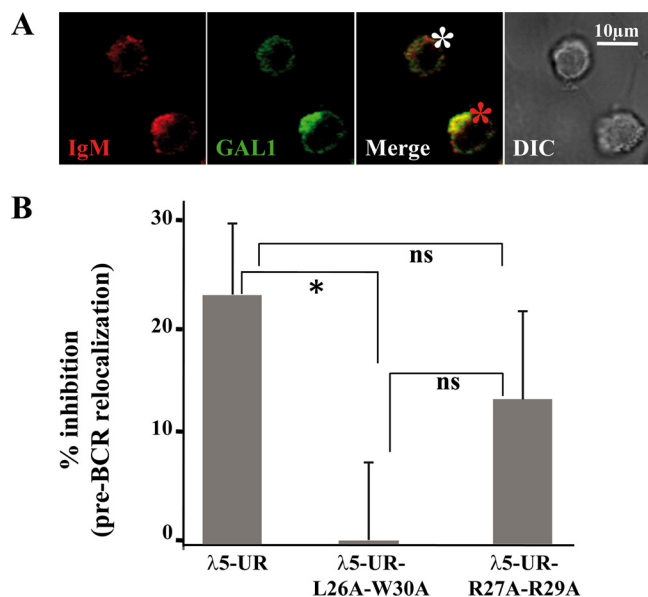


FIGURE 6. Analysis of pre-BCR relocalization. A, Nalm6 pre-B cells were co-cultured on OP9 stromal cells and were analyzed using confocal microscopy. The differential interferential contrast (DIC) image shows fixed pre-B/stromal cell conjugates. The staining was performed using goat anti-human IgM (red) and rabbit anti-GAL1 AS (green) antibodies. The red and the white stars indicate cells with a relocalized and a nonrelocalized pre-BCR, respectively. B, inhibition of pre-BCR relocalization in the presence of the λ5-UR and of the two λ5-UR mutants is shown. Three independent experiments were performed, and the data are expressed as the percentage of inhibition of pre-BCR relocalization ± S.D. (error bars). Pre-BCR relocalization was inhibited 25% in the presence of recombinant λ5-UR. Similar inhibition levels have been reported (7) and were highly significant (p value = 0.008, data not shown). *, $p = 0.018$ between λ5-UR and λ5-UR-L26A/W30A and ns (not significant) between λ5-UR and λ5-UR-R27A/R29A ($p = 0.07$) and between λ5-UR-L26A/W30A and λ5-UR-R27A/R29A ($p = 0.06$).

bic residues are crucial for the pre-BCR relocalization. Surprisingly, pre-BCR relocalization in the presence of the λ5-UR-R27A/R29A mutant is not significantly diminished (Fig. 6B). These results suggest that the charged and the hydrophobic residues tested have not the same contribution on the relocalization process.

To evaluate at a molecular level the importance of the hydrophobic and electrostatic interactions, the effect of replacing the interacting residues on the formation of the complex was tested using NMR (supplemental Figs. S5 and S6). To target the hydrophobic core of the complex, we used two complementary mutants, GAL1-Y104A/F106A and λ5-UR²²⁻⁴⁵-L26A/W30A. The effect of the hydrophobic substitutions was significant, resulting in a strong impairment of the complex formation (supplemental Fig. S6, B and C). We also targeted the two electrostatic contacts participating in the complex formation using the GAL1-E74A/D102A and the λ5-UR²²⁻⁴⁵-R27A/R29A mutants. These mutations had a lesser effect on the complex formation (supplemental Fig. S6, D and E), as suggested by the results from the pre-BCR relocalization assays (Fig. 6B). Therefore, the pre-BCR relocalization and the NMR experiments show that the GAL1/pre-BCR complex formation and the GAL1-induced pre-BCR relocalization are hydrophobically driven with a minor contribution from electrostatic contacts.

DISCUSSION

We have identified a minimal GAL1-interacting region within the 45 residues of the full-length λ5-UR. One important finding of our study is that the central region (residues 29–39) adopts a stable helical conformation, which preexists in solution prior binding to GAL1 (Fig. 3). It is so far the first detailed structural information about the λ5-UR. Structural data of the human GAL1 in complex with λ5-UR²²⁻⁴⁵ (Fig. 4) revealed that the central feature of the binding is the involvement of the λ5-UR²²⁻⁴⁵ α-helix over its entire length in the interaction with the GAL1 binding surface. Complex formation is mainly mediated by hydrophobic residues present on both partners and, at a lower extent, by electrostatic contacts involving two arginines on λ5-UR²²⁻⁴⁵ and two acidic residues on GAL1. Moreover, we found that the hydrophobic contribution to GAL1/λ5 complex formation is critical for pre-BCR relocalization when pre-B cells are co-cultured with GAL1⁺ stromal cells (Fig. 6), validating our structural data in a biological context. These results represent the first atomic view of a pre-BCR/ligand interaction.

Besides its carbohydrate binding activity, GAL1 has also been described as being engaged in protein interactions in a carbohydrate-independent manner (13). These interactions occur mainly in the intracellular compartments whereas its carbohydrate binding activity is mostly extracellular. So far, the λ5 protein from the pre-BCR is a unique example of a nonglycosylated protein partner of GAL1 described in the extracellular matrix. Among the intracellular nonglycosylated partners of GAL1, actin (25, 26), Gemin4 (27, 28), and Ras (29, 30) involved in a variety of intracellular functions have been identified. These proteins do not share consensus amino acid sequence or structural motifs, and neither the GAL1 sites nor the structural determinants that are involved in these interactions have been established yet. In the case of H-Ras/GAL1 interactions, Rotbalt *et al.* identified a hydrophobic surface on GAL1 possessing isoprenoid-binding residues essential for Ras-GTP stabilization and its association with the membrane (30). This surface, which has been proposed to interact with the farnesyl group of Ras, lies within the GAL1 β-sheet and includes residues Leu-9, Leu-11, Leu-17, Phe-30, Phe-32 and Ile-128. Thus, λ5 interacting surface on GAL1 is different from this proposed Ras farnesyl binding site.

The other feature revealed by our studies is the close proximity of λ5 interacting surface with the CBS on GAL1 (Fig. 4). During synapse formation, GAL1 has a central role by interacting with the pre-BCR through a protein/protein interaction, but also with glycosylated counterreceptors through protein-carbohydrate recognition (8). We have observed that the absence of lactose has no significant effect on λ5-UR²²⁻⁴⁵ binding to GAL1 (Fig. 2A). This is in agreement with our previous observations that there is no direct competition of SLC and carbohydrates for GAL1 binding (8) and that GAL1 is able to interact at the same time with λ5 (protein/protein interaction) and with integrins (protein/carbohydrate interaction) during synapse formation (11). On the other hand, we have shown that λ5-UR²²⁻⁴⁵ binding to GAL1 induces a 4-fold decrease in the lactose binding activity of GAL1 (Fig. 5). Moreover, some residues belonging to GAL1 CBS undergo chemical shift variations

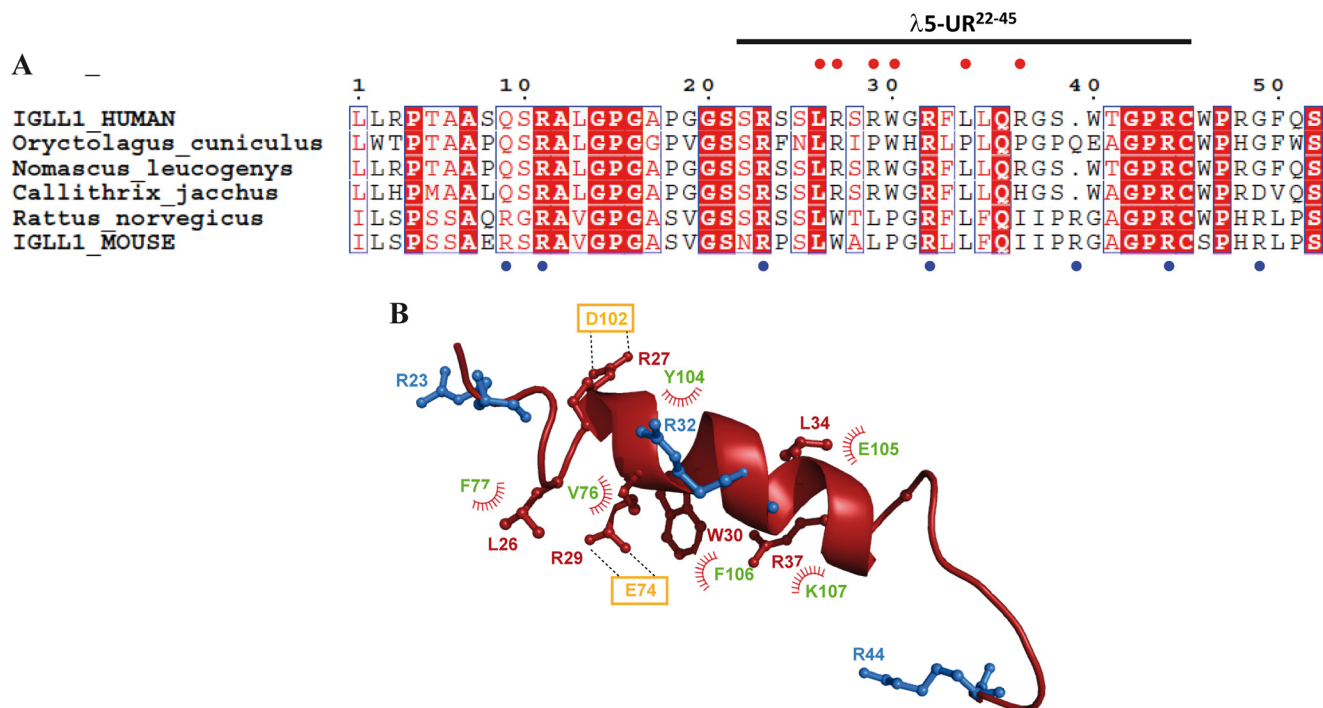


FIGURE 7. **Sequence and structural analysis of λ 5-UR.** *A*, conserved residues of the λ 5-UR sequence in various species are shown in the red boxes. Above the sequences, the residues involved in the GAL1 interaction are labeled with red dots; below the sequences, the λ 5-UR arginines involved in autonomous pre-BCR oligomerization are labeled with blue dots (9). *B*, bound λ 5-UR²²⁻⁴⁵ structure shows λ 5-UR²²⁻⁴⁵ residues interacting with GAL1 colored red, the conserved arginines involved in autonomous pre-BCR oligomerization are colored blue, GAL1 hydrophobic residues are labeled in green, and electrostatic residues are in orange.

upon λ 5-UR²²⁻⁴⁵ binding to GAL1 (Figs. 1D and 2A), suggesting modifications of the CBS upon λ 5 binding.

Another known example of a GAL1/peptide interaction is the binding of the nonnatural peptide Anginex (31). This peptide is a powerful antiangiogenic molecule with antitumor activity because it blocks adhesion and migration of activated endothelial cells thus preventing angiogenesis *in vitro* and *in vivo* (31–33). Recent studies (34) have shown that binding of Anginex to GAL1 greatly enhances the affinity of GAL1 for certain ligands, including biologically relevant glycoproteins. Moreover, a topomimetic of Anginex has been shown to be an allosteric inhibitor of GAL1 lactose binding while interacting with a surface of GAL1 located on the back face of the protein (35). This implies that Anginex could have opposite effect on GAL1 depending on the carbohydrate substrate tested. In our system, the exact oligosaccharide ligands of GAL1 at the cell surface of stromal and pre-BII cells have not been identified. Thus, it is not excluded that λ 5-UR could have an effect similar to that of Anginex on GAL1 at the synapse. Indeed, modulation of GAL1 affinity for specific glycoproteins, either enhanced or reduced, could be a strategic step at the synapse level to modify the cross-linked lattices. These modifications of the interacting network could be crucial during pre-BCR oligomerization and subsequent receptor internalization.

The sequence analysis emphasizes that the GAL1 hydrophobic and charged amino acids involved in the λ 5 interacting site are highly conserved among species (supplemental Fig. S7). Similarly, the human and primate λ 5 sequences are well conserved, although differences in the rat and mouse sequences exist (Fig. 7A). The main difference observed is the replacement

in rat and mouse of the human Arg-27 and Arg-29 by Trp and Leu hydrophobic residues, respectively, thus enhancing the hydrophobic interacting potential of this region. Moreover, we have shown that these two arginines are not critical for pre-BCR relocalization (Fig. 6).

Previous studies in mice revealed a crucial role for conserved λ 5-UR arginines (Arg-9, Arg-11, Arg-23, Arg-32, Arg-39, Arg-44, and Arg-49) in the autonomous pre-BCR oligomerization (9). Indeed, deletion of full-length λ 5-UR or mutations of these conserved arginines led to an increase in pre-BCR cell surface expression and to a decrease in pre-BCR clustering and internalization. Here, the GAL1/ λ 5-UR²²⁻⁴⁵ complex clearly shows that Arg-23, Arg-32, and Arg-44 are not facing the GAL1 interacting surface, but in contrast to the λ 5-UR²²⁻⁴⁵ residues delineating the hydrophobic interacting surface, they are solvent-exposed (Fig. 7B). Our data indicate that from a structural point of view, autonomous and GAL1-induced pre-BCR oligomerizations do not involve the same set of residues; these processes are therefore not in competition and could instead be complementary. However, it remains unclear under which conditions during pre-BII cell differentiation and/or selection of the V_H repertoire a unique activation mode or a combination of both modes is required. A hypothesis could be that constitutive pre-BCR activation which has been recently shown to be very low (36) is helped by the stromal-derived GAL1, hence strengthening the pre-BCR oligomerization leading to synapse formation and optimal pre-BCR activation. The requirement of GAL1 could be linked to the level of pre-BCR surface expression. In the case of a low pre-BCR surface expression, as is mainly the case for normal pre-BII cells *in*

in vivo, GAL1-induced signaling would be required to amplify pre-BCR functions, whereas in the case of a high receptor expression, GAL1 could not be necessary for pre-BCR oligomerization. These studies provide the first molecular snapshot of a pre-BCR/ligand interaction that promotes pre-BCR clustering leading to pre-BCR activation.

Acknowledgments—We thank Caroline Breton for help with the pre-BCR relocalization experiments, Stéphane Mancini for contributions to the statistical analysis, and Corinne Sebban-Kreuzer for help with the K_D calculation. We thank the TGE RMN THC (Très Grands Equipements de Résonance Magnétique Nucléaire à Très Haut Champs) FR3050 for performing the research.

REFERENCES

- Melchers, F. (2005) The pre-B-cell receptor: selector of fitting immunoglobulin heavy chains for the B-cell repertoire. *Nat. Rev. Immunol.* **5**, 578–584
- Kitamura, D., Roes, J., Kühn, R., and Rajewsky, K. (1991) A B cell-deficient mouse by targeted disruption of the membrane exon of the immunoglobulin mu chain gene. *Nature* **350**, 423–426
- ten Boekel, E., Melchers, F., and Rolink, A. (1997) Changes in the V_H gene repertoire of developing precursor B lymphocytes in mouse bone marrow mediated by the pre-B cell receptor. *Immunity* **7**, 357–368
- Keenan, R. A., De Riva, A., Corleis, B., Hepburn, L., Licence, S., Winkler, T. H., and Mårtensson, I. L. (2008) Censoring of autoreactive B cell development by the pre-B cell receptor. *Science* **321**, 696–699
- Bankovich, A., Raunser, S., Juo, Z. S., Walz, T., Davis, M. M., and Garcia, K. C. (2007) Structural insight into pre-B cell receptor function. *Science* **316**, 291–294
- Bradl, H., Wittmann, J., Milius, D., Vettermann, C., and Jäck, H. M. (2003) Interaction of murine precursor B cell receptor with stroma cells is controlled by the unique tail of $\lambda 5$ and stroma cell-associated heparan sulfate. *J. Immunol.* **171**, 2338–2348
- Espeli, M., Mancini, S. J., Breton, C., Poirier, F., and Schiff, C. (2009) Impaired B-cell development at the pre-BII-cell stage in galectin-1-deficient mice due to inefficient pre-BII/stromal cell interactions. *Blood* **113**, 5878–5886
- Gauthier, L., Rossi, B., Roux, F., Termine, E., and Schiff, C. (2002) Galectin-1 is a stromal cell ligand of the pre-B cell receptor (BCR) implicated in synapse formation between pre-B and stromal cells and in pre-BCR triggering. *Proc. Natl. Acad. Sci. U.S.A.* **99**, 13014–13019
- Ohnishi, K., and Melchers, F. (2003) The nonimmunoglobulin portion of $\lambda 5$ mediates cell-autonomous pre-B cell receptor signaling. *Nat. Immunol.* **4**, 849–856
- Meixlperger, S., Köhler, F., Wossning, T., Reppel, M., Müschen, M., and Jumaa, H. (2007) Conventional light chains inhibit the autonomous signaling capacity of the B cell receptor. *Immunity* **26**, 323–333
- Rossi, B., Espeli, M., Schiff, C., and Gauthier, L. (2006) Clustering of pre-B cell integrins induces galectin-1-dependent pre-B cell receptor relocalization and activation. *J. Immunol.* **177**, 796–803
- Mourcin, F., Breton, C., Tellier, J., Narang, P., Chasson, L., Jorquera, A., Coles, M., Schiff, C., and Mancini, S. J. (2011) Galectin-1-expressing stromal cells constitute a specific niche for pre-BII cell development in mouse bone marrow. *Blood* **117**, 6552–6561
- Camby, I., Le Mercier, M., Lefranc, F., and Kiss, R. (2006) Galectin-1: a small protein with major functions. *Glycobiology* **16**, 137R–157R
- Barondes, S. H., Cooper, D. N., Gitt, M. A., and Leffler, H. (1994) Galectins: structure and function of a large family of animal lectins. *J. Biol. Chem.* **269**, 20807–20810
- López-Lucendo, M. F., Solís, D., André, S., Hirabayashi, J., Kasai, K., Kaltner, H., Gabius, H. J., and Romero, A. (2004) Growth-regulatory human galectin-1: crystallographic characterisation of the structural changes induced by single-site mutations and their impact on the thermodynamics of ligand binding. *J. Mol. Biol.* **343**, 957–970
- Pace, K. E., Hahn, H. P., and Baum, L. G. (2003) Preparation of recombinant human galectin-1 and use in T-cell death assays. *Methods Enzymol.* **363**, 499–518
- Dodd, R. B., Allen, M. D., Brown, S. E., Sanderson, C. M., Duncan, L. M., Lehner, P. J., Bycroft, M., and Read, R. J. (2004) Solution structure of the Kaposi's sarcoma-associated herpesvirus K3 N-terminal domain reveals a novel E2-binding C4HC3-type RING domain. *J. Biol. Chem.* **279**, 53840–53847
- Grzesiek, S., Bax, A., Clore, G. M., Gronenborn, A. M., Hu, J. S., Kaufman, J., Palmer, I., Stahl, S. J., and Wingfield, P. T. (1996) The solution structure of HIV-1 Nef reveals an unexpected fold and permits delineation of the binding surface for the SH3 domain of Hck tyrosine protein kinase. *Nat. Struct. Biol.* **3**, 340–345
- Pearlman, D. A., and Connelly, P. R. (1995) Determination of the differential effects of hydrogen bonding and water release on the binding of FK506 to native and Tyr-82 \rightarrow Phe-82 FKBP-12 proteins using free energy simulations. *J. Mol. Biol.* **248**, 696–717
- Laskowski, R. A., Rullmann, J. A., MacArthur, M. W., Kaptein, R., and Thornton, J. M. (1996) AQUA and PROCHECK-NMR: programs for checking the quality of protein structures solved by NMR. *J. Biomol. NMR* **8**, 477–486
- Dominguez, C., Boelens, R., and Bonvin, A. M. (2003) HADDOCK: a protein-protein docking approach based on biochemical or biophysical information. *J. Am. Chem. Soc.* **125**, 1731–1737
- Lanig, H., Bradl, H., and Jäck, H. M. (2004) Three-dimensional modeling of a pre-B-cell receptor. *Mol. Immunol.* **40**, 1263–1272
- Nesmelova, I. V., Pang, M., Baum, L. G., and Mayo, K. H. (2008) ^1H , ^{13}C , and ^{15}N backbone and side-chain chemical shift assignments for the 29 kDa human galectin-1 protein dimer. *Biomol. NMR Assign.* **2**, 203–205
- Nesmelova, I. V., Ermakova, E., Daragan, V. A., Pang, M., Menéndez, M., Lagartera, L., Solís, D., Baum, L. G., and Mayo, K. H. (2010) Lactose binding to galectin-1 modulates structural dynamics, increases conformational entropy, and occurs with apparent negative cooperativity. *J. Mol. Biol.* **397**, 1209–1230
- Joubert, R., Caron, M., Avellana-Adalid, V., Mornet, D., and Bladier, D. (1992) Human brain lectin: a soluble lectin that binds actin. *J. Neurochem.* **58**, 200–203
- Camby, I., Belot, N., Lefranc, F., Sadeghi, N., de Launoit, Y., Kaltner, H., Musette, S., Darro, F., Danguy, A., Salmon, I., Gabius, H. J., and Kiss, R. (2002) Galectin-1 modulates human glioblastoma cell migration into the brain through modifications to the actin cytoskeleton and levels of expression of small GTPases. *J. Neuropathol. Exp. Neurol.* **61**, 585–596
- Park, J. W., Voss, P. G., Grabski, S., Wang, J. L., and Patterson, R. J. (2001) Association of galectin-1 and galectin-3 with Gemin4 in complexes containing the SMN protein. *Nucleic Acids Res.* **29**, 3595–3602
- Vyakarnam, A., Dagher, S. F., Wang, J. L., and Patterson, R. J. (1997) Evidence for a role for galectin-1 in pre-mRNA splicing. *Mol. Cell. Biol.* **17**, 4730–4737
- Paz, A., Haklai, R., Elad-Sfadia, G., Ballan, E., and Kloog, Y. (2001) Galectin-1 binds oncogenic H-Ras to mediate Ras membrane anchorage and cell transformation. *Oncogene* **20**, 7486–7493
- Rotblat, B., Niv, H., André, S., Kaltner, H., Gabius, H. J., and Kloog, Y. (2004) Galectin-1(L11A) predicted from a computed galectin-1 farnesyl-binding pocket selectively inhibits Ras-GTP. *Cancer Res.* **64**, 3112–3118
- Thijssen, V. L., Postel, R., Brandwijk, R. J., Dings, R. P., Nesmelova, I., Satijn, S., Verhofstad, N., Nakabepu, Y., Baum, L. G., Bakkers, J., Mayo, K. H., Poirier, F., and Griffioen, A. W. (2006) Galectin-1 is essential in tumor angiogenesis and is a target for antiangiogenesis therapy. *Proc. Natl. Acad. Sci. U.S.A.* **103**, 15975–15980
- Griffioen, A. W., van der Schaft, D. W., Barendsz-Janson, A. F., Cox, A., Struijker Boudier, H. A., Hillen, H. F., and Mayo, K. H. (2001) Anginex, a designed peptide that inhibits angiogenesis. *Biochem. J.* **354**, 233–242
- van der Schaft, D. W., Dings, R. P., de Lussanet, Q. G., van Eijk, L. I., Nap, A. W., Beets-Tan, R. G., Bouma-Ter Steege, J. C., Wagstaff, J., Mayo, K. H., and Griffioen, A. W. (2002) The designer anti-angiogenic peptide anginex targets tumor endothelial cells and inhibits tumor growth in animal models. *FASEB J.* **16**, 1991–1993

34. Salomonsson, E., Thijssen, V. L., Griffioen, A. W., Nilsson, U. J., and Leffler, H. (2011) The anti-angiogenic peptide anginex greatly enhances galectin-1 binding affinity for glycoproteins. *J. Biol. Chem.* **286**, 13801–13804
35. Dings, R. P., Miller, M. C., Nesselova, I., Astorgues-Xerri, L., Kumar, N., Serova, M., Chen, X., Raymond, E., Hoye, T. R., and Mayo, K. H. (2012) Antitumor agent calixarene 0118 targets human galectin-1 as an allosteric inhibitor of carbohydrate binding. *J. Med. Chem.* **55**, 5121–5129
36. Knoll, M., Yanagisawa, Y., Simmons, S., Engels, N., Wienands, J., Melchers, F., and Ohnishi, K. (2012) The non-Ig parts of the VpreB and $\lambda 5$ proteins of the surrogate light chain play opposite roles in the surface representation of the precursor B cell receptor. *J. Immunol.* **188**, 6010–6017

Structural Basis for Galectin-1-dependent Pre-B Cell Receptor (Pre-BCR) Activation

Latifa Elantak, Marion Espeli, Annie Boned, Olivier Bornet, Jeremy Bonzi, Laurent Gauthier, Mikael Feracci, Philippe Roche, Françoise Guerlesquin and Claudine Schiff

J. Biol. Chem. 2012, 287:44703-44713.

doi: 10.1074/jbc.M112.395152 originally published online November 2, 2012

Access the most updated version of this article at doi: [10.1074/jbc.M112.395152](https://doi.org/10.1074/jbc.M112.395152)

Alerts:

- [When this article is cited](#)
- [When a correction for this article is posted](#)

[Click here](#) to choose from all of JBC's e-mail alerts

Supplemental material:

<http://www.jbc.org/content/suppl/2012/11/02/M112.395152.DC1>

This article cites 36 references, 14 of which can be accessed free at <http://www.jbc.org/content/287/53/44703.full.html#ref-list-1>

SUPPLEMENTAL DATA

Table S1. Primers used for the constructions of recombinant GAL1 and λ 5 mutants

	Sense primer (5' to 3')	Anti-sense primer (5' to 3')
GAL1 mutants		
GAL1-E74A	ccgagcagcgggagggtgtttcc	ggaaagacagccgccgctgctcgg
GAL1-D102A	gaccgtcaagctgccagcgggatacgaattcaagtc	gaacttgaattcgtatcccgtggcagcttgacggtc
GAL1-Y104A-F106A	cagatggagccgaagccaagtccccaac	gttggggaactggcttcggctccatctg
λ5-UR-WT (for pET28a cloning)	aaaggatcctcgcagagcaggg	aaactcgagtcattaatgcgtcactgagttatg
λ5-UR-GST mutants		
λ5-UR-L26A-W30A-GST	ccggtccagcgcgaggagccggggggcagggttc	gaacctgccccccggctcctcgcgctggaccgg
λ5-UR-R27A-R29A-GST	ccggtccagcctggcgagcgcgtggggcagggttc	gaacctgccccacgcgctcggcaggtggaccgg

Table S2. NMR statistics for the λ 5-UR²²⁻⁴⁵ structures

	Free	GAL1-bound
Total NOE distance limits	231	318
Short-range, $ i-j \leq 1$	182	251
Medium-range, $1 < i-j < 5$	49	60
Long-range, $ i-j \geq 5$	0	7
Violations (mean \pm sd)		
Number of distance violations $> 0.5 \text{ \AA}$	2	6
Max. distance constraint violation (\AA)	0.66	1.4
Ramachandran statistics		
Most favorable regions (%)	72.7	48.2
Additional allowed regions (%)	22.7	46.1
Generously allowed regions (%)	4.5	5.1
Disallowed regions (%)	0.0	0.6
Average pairwise rmsd (\AA) for residues 25-41		
Heavy (to mean)	0.89 ± 0.07 (2.0 \AA for all residues)	0.93 ± 0.11 (2.2 \AA for all residues)
Backbone (to mean)	0.17 ± 0.07 (1.3 \AA for all residues)	0.58 ± 0.13 (1.7 \AA for all residues)

SUPPLEMENTAL FIGURE LEGENDS

Figure S1: (A) Schematic representation of the different regions of the human $\lambda 5$ protein. (B) Amino acid sequence of the $\lambda 5$ -UR used in this study is shown below. The protein numbering is as found in the UniProtKB database under the accession code P15814. Previous studies identified the first residue of the mature protein as Ser 8 (1). (C) The theoretical prediction of helical percentage for $\lambda 5$ -UR as a function of residue number was performed using the AGADIR algorithm (2). (D) Circular dichroism spectrum of $\lambda 5$ -UR. Circular dichroism (CD) spectra were recorded on a Jasco 815 CD spectrometer using 2 mm path length quartz cells in PBS 1X at 20 °C. CD spectra were measured from 260 to 190 nm and were averaged from four scans.

Figure S2: ^1H - ^{15}N HSQC spectra of ^{15}N -labelled GAL1 (0.3 mM) free of lactose, in the absence (black peaks) and the presence of 1 molar equivalent of (A) $\lambda 5$ -UR $^{22-45}$ peptide (red peaks) and (B) full-length $\lambda 5$ -UR (pink peaks).

Figure S3: Sequential nOes extracted from NOESY spectra for (A) the free $\lambda 5$ -UR $^{22-45}$ peptide and (B) for the GAL1-bound $\lambda 5$ -UR $^{22-45}$ peptide.

Figure S4: Intermolecular nOes within the GAL1/ $\lambda 5$ -UR $^{22-45}$ complex. Comparison of regions extracted from 2D ^{15}N , ^{13}C – filtered NOESY (black peaks) and 2D ^{15}N , ^{13}C – half-filtered NOESY (red peaks) spectra recorded on the ^{15}N , ^{13}C – GAL1/ $\lambda 5$ -UR $^{22-45}$ sample. In the 2D ^{15}N , ^{13}C -filtered NOESY spectrum, only the intramolecular correlations of the unlabelled $\lambda 5$ -UR $^{22-45}$ are detected whereas in the 2D ^{15}N , ^{13}C – half-filtered NOESY spectrum intramolecular correlations within the $\lambda 5$ -UR $^{22-45}$ and intermolecular correlations between $\lambda 5$ -UR $^{22-45}$ and the labeled ^{15}N - ^{13}C -GAL1 are detected. Overlay of both spectra thus highlights the intermolecular correlations. On the basis of the $\lambda 5$ -UR $^{22-45}$ peptide and GAL1 resonance assignments that we

performed on the complexed forms, 10 intermolecular nOe restraints have been assigned in the half-filtered NOESY spectra recorded on ^{15}N - ^{13}C -GAL1/ $\lambda 5$ -UR²²⁻⁴⁵ complex. Eight of the ten intermolecular nOe correlations between GAL1 and $\lambda 5$ -UR²²⁻⁴⁵ used for structure calculations of the complex are annotated (primed number correspond to $\lambda 5$ -UR²²⁻⁴⁵ resonances). Sample concentrations were 0.7 mM for the GAL1 monomer with the $\lambda 5$ -UR²²⁻⁴⁵ peptide added up to a final concentration of 0.88 mM.

Figure S5: ^1H - ^{15}N HSQC spectra of ^{15}N -labeled GAL1-wt (**A**), ^{15}N -GAL1-Y104A-F106A (**B**), and ^{15}N -GAL1-E74A-D102A (**C**) in the presence of 2 molar excess of $\lambda 5$ -UR²²⁻⁴⁵ are shown. ^1H - ^{15}N HSQC spectra of ^{15}N -labeled GAL1-wt in the presence of 2 molar excess $\lambda 5$ -UR²²⁻⁴⁵-L26A-W30A or $\lambda 5$ -UR²²⁻⁴⁵-R27A-R29A are shown in (**D**) and (**E**), respectively.

Figure S6: (**A**) Chemical shift variations of ^{15}N -labelled GAL1 in the presence of $\lambda 5$ -UR²²⁻⁴⁵ (same as in Fig. 2A) are shown. Chemical shift variations of ^{15}N -labelled GAL1-Y104A-F106A, and GAL1-E74A-D102A in the presence of 2 molar excess of $\lambda 5$ -UR²²⁻⁴⁵ are shown in (**B**) and (**D**), respectively. Chemical shift variations of ^{15}N -labelled GAL1 in the presence of 2 molar excess of $\lambda 5$ -UR²²⁻⁴⁵-L26A-W30A and $\lambda 5$ -UR²²⁻⁴⁵-R27A-R29A are shown in (**C**) and (**E**), respectively. For each experiment, the corresponding chemical shift variation plot is shown as grey bars. For GAL1 mutants, grey stars indicate the residues with missing NH peaks, and red stars represent the mutation location. The plots are color-coded according to the location of the residues on GAL1, as shown in Fig. 2.

Figure S7: (**A**) Alignment of GAL1 sequences from different species. The numbering corresponds to the human GAL1 sequence. The secondary structures of human GAL1 are shown above the sequences. (**B**) Sequence conservation of GAL1 mapped onto the GAL1 surface was calculated using the ConSurf server (<http://consurf.tau.ac.il/>). Delineation of the $\lambda 5$ -UR²²⁻⁴⁵-interacting surface is represented by a dashed line.

REFERENCES

1. Guelpa-Fonlupt, V., Bossy, D., Alzari, P., Fumoux, F., Fougereau, M., and Schiff, C. (1994) The human pre-B cell receptor: structural constraints for a tentative model of the pseudo-light (psi L) chain. *Mol Immunol* **31**, 1099-1108
2. Muñoz, V., and Serrano, L. (1994) Elucidating the folding problem of helical peptides using empirical parameters. *Nat Struct Biol* **1**, 399-409

Figure S1

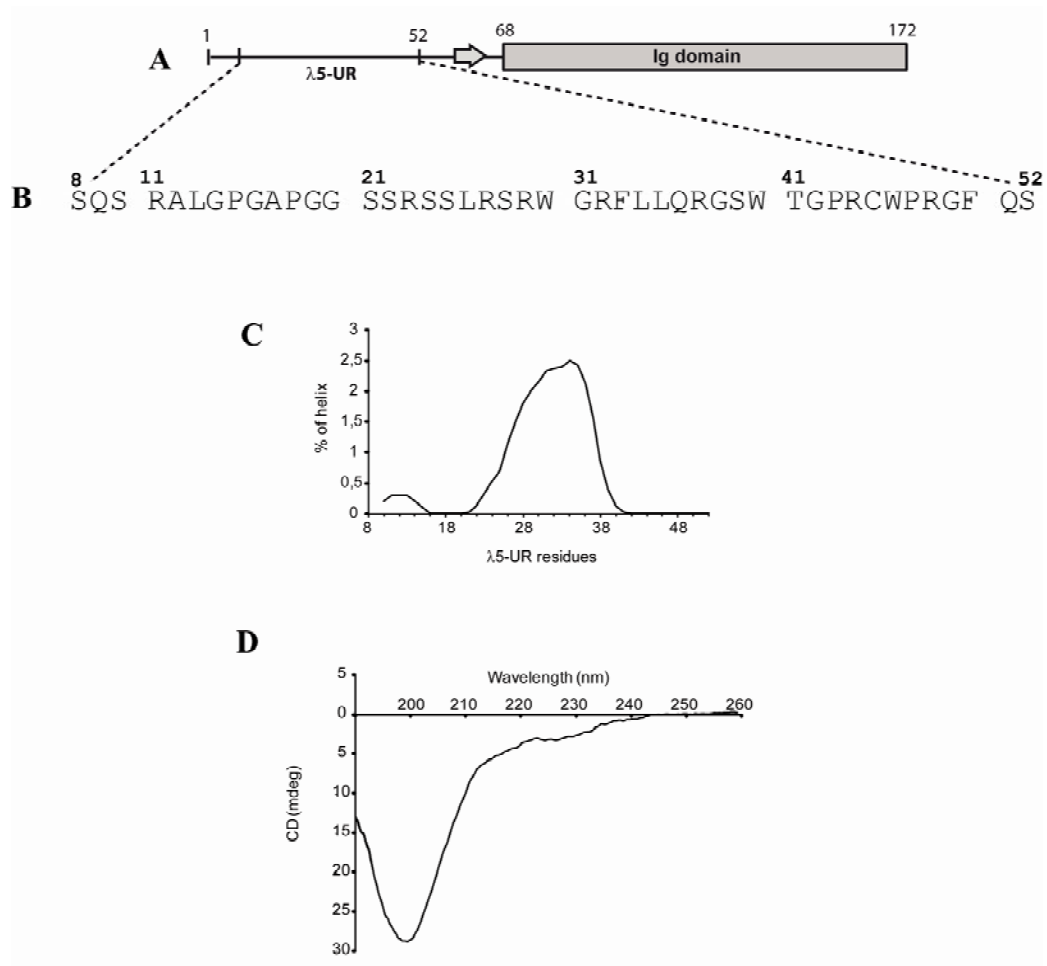


Figure S2

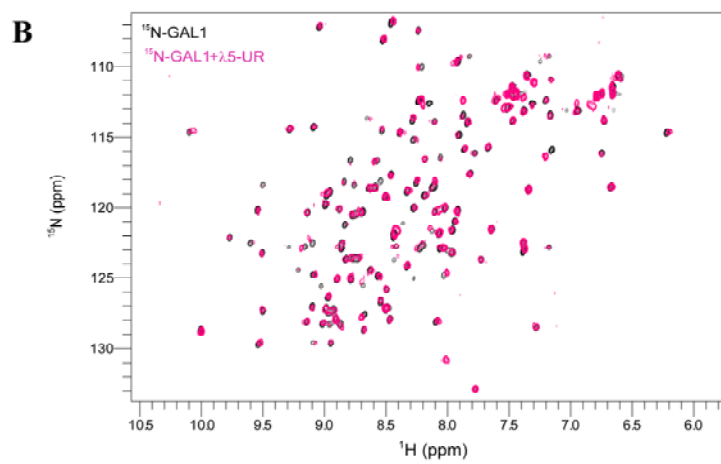
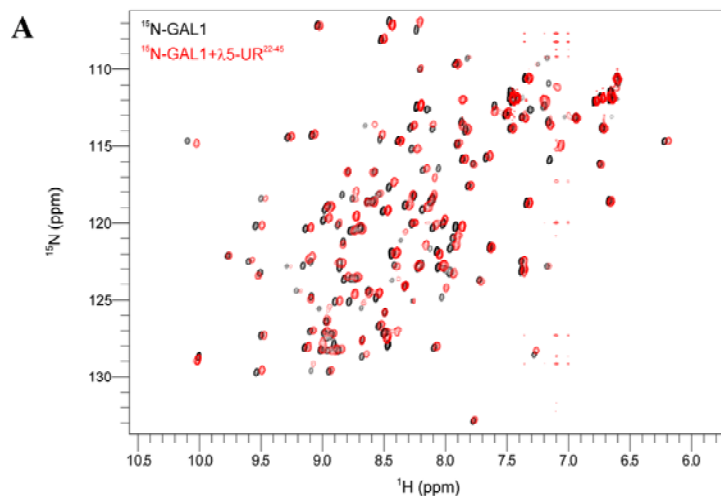


Figure S4

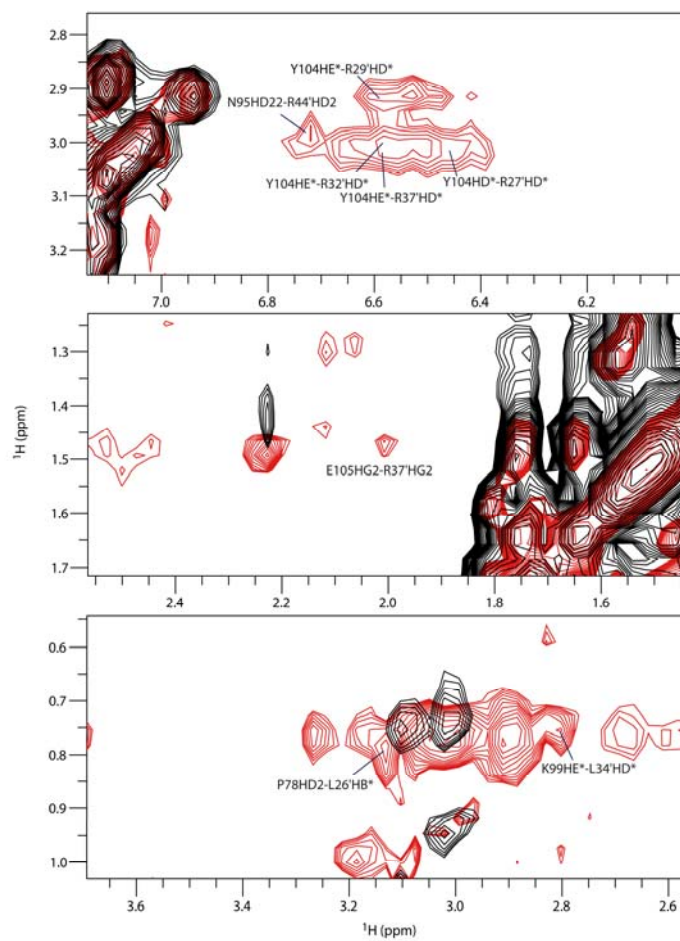


Figure S5

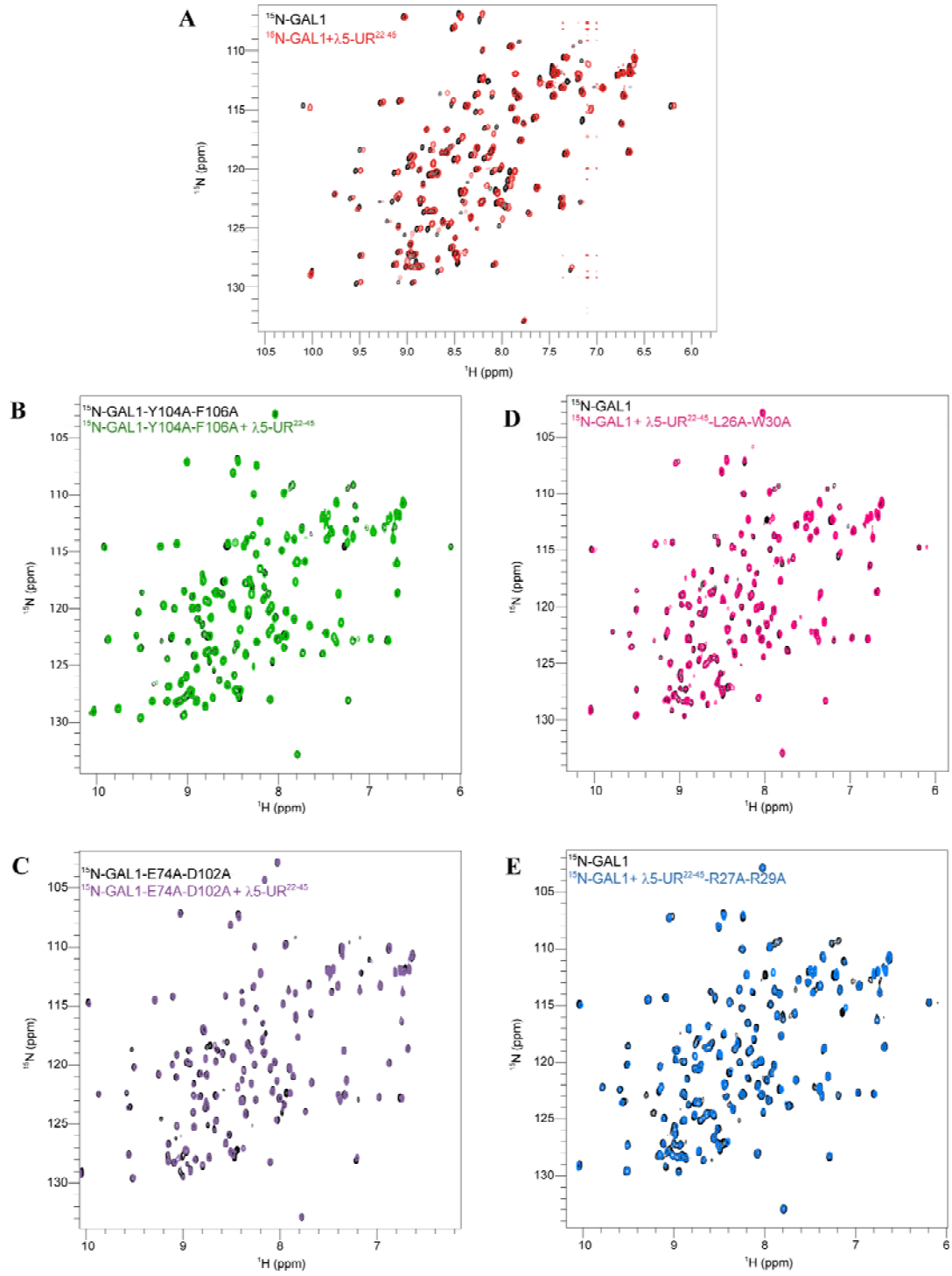


Figure S6

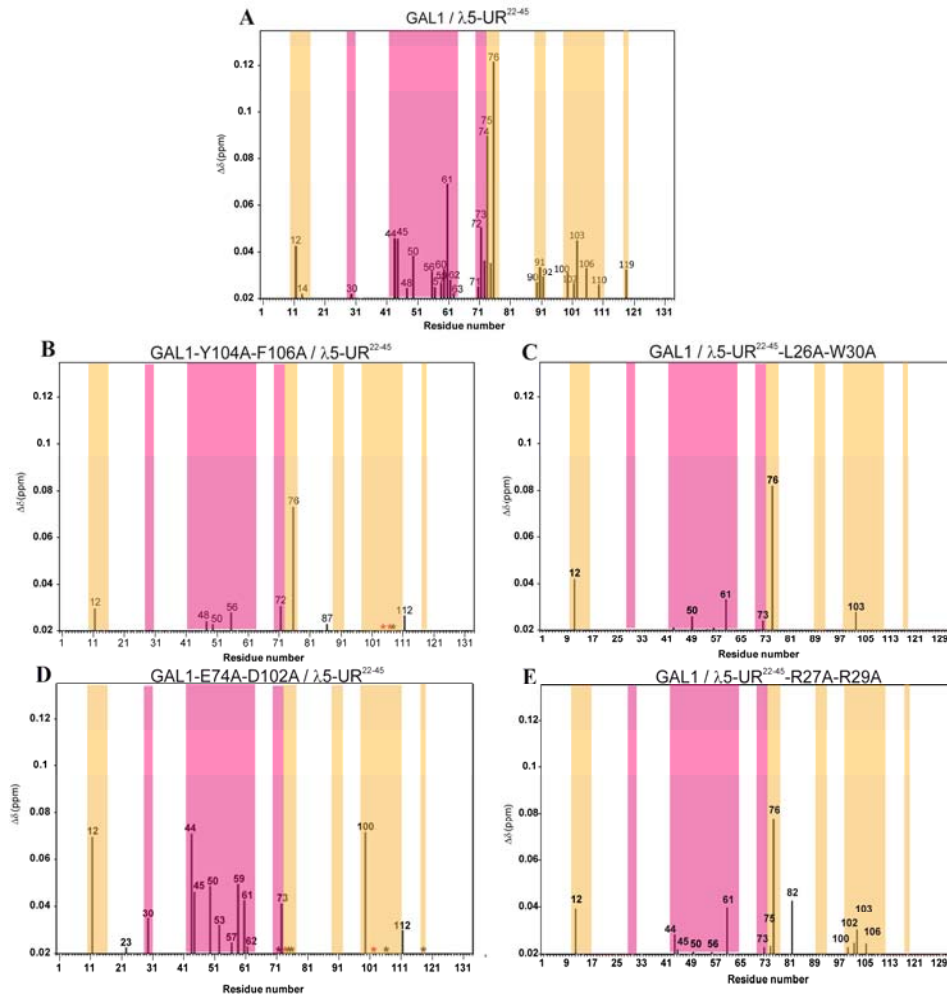
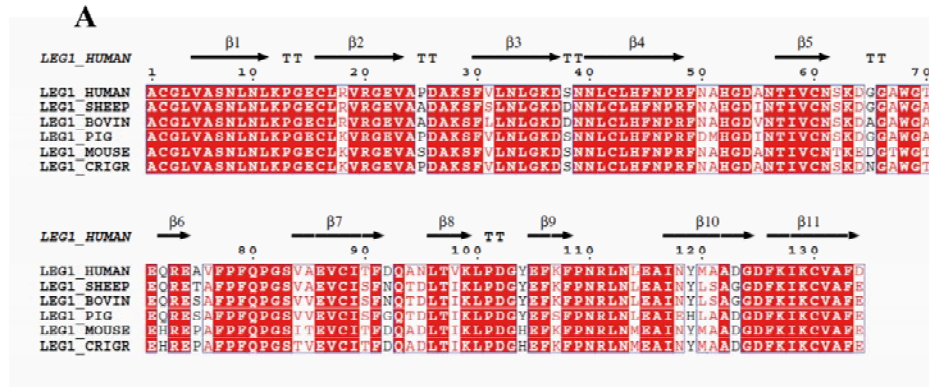
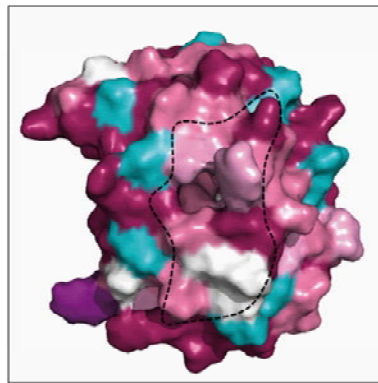


Figure S7



B



1 2 3 4 5 6 7 8 9
 Variable Average Conserved